

## Accurate Sampling of High-Frequency Motions in Proteins by Steady-State $^{15}\text{N}$ – $\{^1\text{H}\}$ Nuclear Overhauser Effect Measurements in the Presence of Cross-Correlated Relaxation

Fabien Ferrage,<sup>\*,†,‡</sup> David Cowburn,<sup>†</sup> and Ranajeet Ghose<sup>§,||</sup>

New York Structural Biology Center, New York, New York 10027, Département de Chimie, Ecole Normale Supérieure, and U.M.R 7203, C.N.R.S., Paris, France, Department of Chemistry, City College of the City University of New York, New York 10031, and Graduate Center of the City University of New York, New York 10016

Received December 5, 2008; E-mail: Fabien.Ferrage@ens.fr

Dynamics are essential for protein function. Fast motions that are important for protein interactions<sup>1</sup> can also be linked to slower motions involved in enzyme catalysis.<sup>2</sup> The measurement of backbone  $^{15}\text{N}$  relaxation rates in NMR has become a routine procedure<sup>3,4</sup> to characterize fast local motions.<sup>5,6</sup> These measurements can be complemented by other relaxation data to obtain a more refined view of backbone dynamics.<sup>7</sup> Usually, the  $^{15}\text{N}$  relaxation rates employed to characterize fast protein dynamics are the longitudinal relaxation rate  $R_1$ , the transverse relaxation rate  $R_2$ , and the dipolar cross-relaxation rate between the  $^{15}\text{N}$  and  $^1\text{H}$  nuclei.<sup>8</sup> The last of these rates is essential for the accurate estimation of the spectral density function at high frequency<sup>5,9</sup> and crucial for the identification of fast backbone motions.<sup>10,11</sup> This rate is derived from what is commonly called the “NOE experiment” where the ratio between the steady-state longitudinal  $^{15}\text{N}$  polarization under  $^1\text{H}$  irradiation and at equilibrium without any perturbation is measured.<sup>8,12</sup> The saturation of  $^1\text{H}$ 's is more difficult to achieve than previously assumed, and cross-correlated relaxation<sup>13</sup> affects the steady-state  $^{15}\text{N}$  polarization during  $^1\text{H}$  irradiation. We quantify these errors for the  $^1\text{H}$  irradiation scheme commonly used in the “NOE experiment” and show that they can be suppressed in a straightforward manner, leading to more accurate measurements of spectra density at high frequency.

Several schemes have been proposed for  $^1\text{H}$  irradiation in steady-state NOE experiments. Although composite pulse decoupling<sup>15</sup> can be used, the most common procedure applies a series of pulses and delays.<sup>12,14</sup> Pulses with a variety of flip angles have been advocated,<sup>14</sup> and schemes with  $120^\circ$  pulses are the most popular, based on empirical observations.<sup>16</sup> Surprisingly, theoretical and experimental studies of irradiation schemes are sparse.<sup>14,17</sup> We have recently shown that the symmetry of the saturation scheme is important.<sup>11</sup> Here, we reexamine the accuracy of the experiment as a function of the  $^1\text{H}$  saturation scheme utilizing the Homogeneous Liouville Equation formalism.<sup>17,18</sup>

All experiments were performed on a 600 MHz Bruker Avance spectrometer equipped with a room-temperature probe, using a sample of perdeuterated and  $^{15}\text{N}$ -labeled human ubiquitin (0.5 mM, in 50 mM ammonium acetate, 300 mM NaCl, pH 4.8). We measured  $^{15}\text{N}\{^1\text{H}\}$  Overhauser effects using a symmetric proton irradiation scheme composed of repeated elements [delay  $\tau/2$  –  $\beta$  pulse – delay  $\tau/2$ ]<sub>*n*</sub>. Experiments were performed with flip angles  $\beta = 90^\circ$ ,  $120^\circ$ , and  $180^\circ$ . In Figure 1a, we show differences,  $\Delta(\beta_1, \beta_2)$ , in the NOE ratio (of intensities with and without  $^1\text{H}$  irradiation) obtained with different flip angles  $\beta$ . Deviations are significant with  $\beta = 120^\circ$  and maximal for  $\beta = 90^\circ$ . As highlighted by color in Figure 1a (e.g., blue points appear on a blue

background), the deviations are a periodic function of the  $^1\text{H}$  carrier frequency, with a period of 200 Hz, which corresponds to the inverse of the interval between two pulses  $\tau$ . A 100 Hz shift of the  $^1\text{H}$  carrier leads to an inversion of all deviations, i.e., to a phase shift  $\pi$  of the periodic function. This observation is rationalized by numerical simulations (Figure 1b).

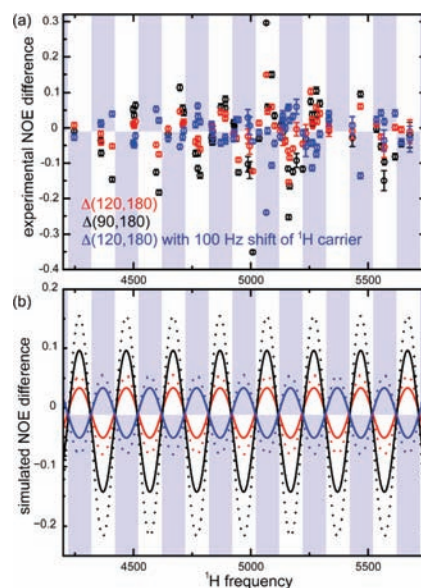


**Figure 1.** (a) Experimentally observed deviations of the NOE ratio,  $\Delta(\beta, 180)$  for rigid NH pairs measured with  $\beta = 120^\circ$  (red);  $\beta = 90^\circ$  (black); and  $\beta = 120^\circ$  (blue) with the  $^1\text{H}$  carrier frequency shifted by 100 Hz from 2820 to 2720 Hz. The blue boxes illustrate the periodic oscillation with a 200 Hz period. (b) Numerical calculations of the deviations of the NOE ratio for a rigid NH pair (solid lines) and a more mobile NH pair (dotted lines), taking CSA/DD cross-correlation into account, color coded as in (a). The delay  $\tau = 5$  ms in the experiments with  $\beta \neq 180^\circ$  and  $\tau = 50$  ms for  $\beta = 180^\circ$ . See Supporting Information (SI) for details about the pulse sequence and numerical calculations.

Figure 1b shows that the calculated steady state  $^{15}\text{N}$  polarization depends on the  $^1\text{H}$  carrier frequency, with a period equal to the inverse of the interpulse delay:  $1/(\tau) = 200$  Hz for  $\tau = 5$  ms. The oscillations can only be reproduced when the cross-correlation of the  $^{15}\text{N}$  chemical shift anisotropy (CSA) and the  $^{15}\text{N}$ – $^1\text{H}$  dipolar coupling is included in simulations.

The oscillations seen in Figure 1 stem from a superposition of two separate effects. The dominant one is largest when the evolution under the offset from the  $^1\text{H}$  carrier and the heteronuclear scalar coupling leads to the conversion  $H_y \rightarrow 2H_yN_z$  during the interpulse delay  $\tau$ . If  $\beta = 90^\circ$ , the sequence  $\beta - \tau - \beta$  leads to the conversion  $H_z \rightarrow -2H_zN_z$ . Subsequent cross-correlated cross-relaxation between

<sup>†</sup> New York Structural Biology Center.

<sup>‡</sup> Ecole Normale Supérieure, and U.M.R 7203, C.N.R.S.

<sup>§</sup> City College of CUNY.

<sup>||</sup> Graduate Center of CUNY.

$2H_zN_z$  and  $N_z$  results in an effective cross-relaxation pathway between the longitudinal polarization operators  $H_z$  and  $N_z$  that perturbs the steady state. The second effect is best observed when the dominant effect vanishes, i.e., when the delay  $\tau$  is a multiple of  $1/|J_{\text{NH}}|$ . The average component  $H_z^{\text{av}}$  vanishes if the  $^1\text{H}$  polarization precesses an integer number of full rotations during the delay  $\tau$ , i.e., at the DANTE condition.<sup>19</sup> Otherwise, the polarization  $H_z$  is not effectively saturated ( $H_z^{\text{av}} \neq 0$ ) so that the  $^{15}\text{N}$  polarization does not evolve toward the desired steady state.

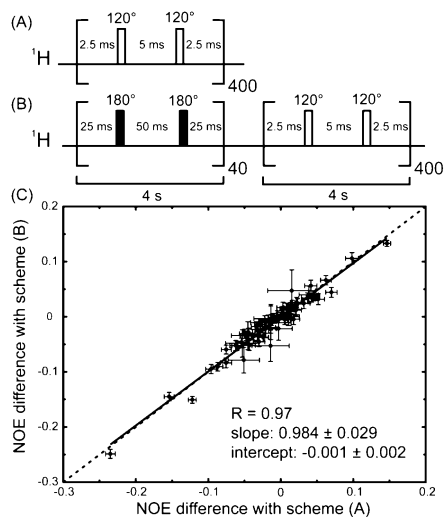


**Figure 2.** Spin-temperature jump experiment using a  $^1\text{H}$  irradiation scheme with  $\beta = 120^\circ$  pulses. (A) Starting right after the FID, and (B) starting from a steady state obtained with  $\beta = 180^\circ$  pulses. (C) Correlations of deviations in the NOE ratios obtained using schemes (A) and (B) with those using  $\beta = 180^\circ$  pulses for 4 s.

To illustrate the validity of this analysis, consider the experiment described in Figure 2, a “spin-temperature jump”, demonstrating that a scheme like (A) creates a steady state different from the steady state obtained with  $180^\circ$  pulses. Intuitively, one might suppose that proton irradiation with any scheme would lead to proper saturation if applied long enough with sufficient power, so that both irradiation schemes would lead to the same steady state. However, as shown in Figure 2, under a sequence of  $120^\circ$  pulses, the polarization  $N_z$  evolves from the “ideal”  $^{15}\text{N}$  steady state (achieved after a 4s irradiation with  $180^\circ$  pulses) toward the same state as the one obtained with scheme (A). Deviations measured under scheme (A) correspond to a different steady state and not to a transient effect.

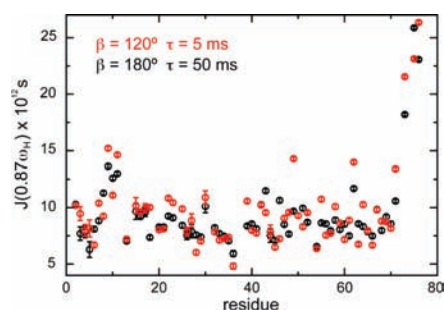


**Figure 3.** Apparent spectral density function  $J(0.87\omega_{\text{H}})$ ,  $\omega_{\text{H}}$  being the  $^1\text{H}$  Larmor frequency, for backbone NH groups in human ubiquitin derived from longitudinal relaxation rates and different sets of NOEs.

Figure 3 shows how systematic errors due to imperfect saturation propagate to the derived spectral density function at high frequency.<sup>12</sup> This value is essential to the quantitative analysis of relaxation data.<sup>3,20</sup>

Deviations in the NOE ratios are amplified, so that large deviations are observed (with a maximum of 47% for Gln49; see SI). When an improper irradiation scheme is used, qualitative interpretations may be biased; for example, high-frequency motions seem to vary significantly in the  $\beta$ -hairpin comprising residues 9–11, while they appear to be uniform with the correct saturation scheme.

In conclusion, we have shown that the steady state  $^{15}\text{N}$  polarization in NOE experiments depends on the flip angle  $\beta$  employed in the saturation sequence. Widely used trains of  $120^\circ$  pulses do not lead to the ideal steady state because of CSA/DD cross-correlated relaxation. Flip angles  $\beta$  should be set to  $180^\circ$  and delays  $\tau$  to integer multiples of the inverse of the scalar coupling  $^1J_{\text{NH}}$ . Improper irradiation leads to significant errors in the estimate of the spectral density functions at high frequency. This effect may be comparable to experimental errors in many studies with low-precision NOE ratios and occurs whether a protein is deuterated or not (SI).

**Acknowledgment.** We thank Geoffrey Bodenhausen and Philippe Pelupessy for their careful reading of the manuscript. We acknowledge support from grants NSF MCB-0347100,0843141 (R.G.), NIH GM 47021(D.C.) and NIH, 5G12 RR06030 (CCNY).

**Supporting Information Available:** Pulse sequence; NOE ratios; relative errors in  $J(0.87\omega_{\text{H}})$ ; NOE deviations (i) with various delays  $\tau$  and (ii) in protonated ubiquitin; simulations of the effect of the size of the protein; propagation of errors to microdynamic parameters; details of numerical calculations. This material is available free of charge via the Internet at <http://pubs.acs.org>.

## References

- Frederick, K. K.; Marlow, M. S.; Valentine, K. G.; Wand, A. J. *Nature (London)* **2007**, *448*, 325–329. Showalter, S. A.; Bruschiweiler-Li, L.; Johnson, E.; Zhang, F.; Bruschiweiler, R. *J. Am. Chem. Soc.* **2008**, *130*, 6472–6478. Dhulesia, A.; Gsponer, J.; Vendruscolo, M. *J. Am. Chem. Soc.* **2008**, *130*, 8931–8939.
- Henzler-Wildman, K. A.; Lei, M.; Thai, V.; Kerns, S. J.; Karplus, M.; Kern, D. *Nature (London)* **2007**, *450*, 913–U27.
- Kay, L. E.; Torchia, D. A.; Bax, A. *Biochemistry* **1989**, *28*, 8972–8979.
- Palmer, A. G. *Chem. Rev.* **2004**, *104*, 3623–3640.
- Farrow, N. A.; Zhang, O. W.; Szabo, A.; Torchia, D. A.; Kay, L. E. *J. Biomol. NMR* **1995**, *6*, 153–162.
- Butterwick, J. A.; Loria, J. P.; Astrof, N. S.; Kroenke, C. D.; Cole, R.; Rance, M.; Palmer, A. G. *J. Mol. Biol.* **2004**, *339*, 855–871.
- Lieninp, S. F.; Bremi, T.; Brutscher, B.; Brüschweiler, R.; Ernst, R. R. *J. Am. Chem. Soc.* **1998**, *120*, 9870–9879. Wang, T. Z.; Cai, S.; Zuiderweg, E. R. P. *J. Am. Chem. Soc.* **2003**, *125*, 8639–8643. Ferrage, F.; Pelupessy, P.; Cowburn, D.; Bodenhausen, G. *J. Am. Chem. Soc.* **2006**, *128*, 11072–11078.
- Cavanagh, J.; Fairbrother, W. J.; Palmer, A. G., III; Rance, M.; Skelton, N. J. *Protein NMR Spectroscopy: Principles and practice*; Academic Press: San Diego, 2006.
- Peng, J. W.; Wagner, G. *J. Magn. Reson.* **1992**, *98*, 308–332. Hansen, D. F.; Yang, D. W.; Feng, H. Q.; Zhou, Z.; Wiesner, S.; Bai, Y. W.; Kay, L. E. *J. Am. Chem. Soc.* **2007**, *129*, 11468–11479.
- Chang, S. L.; Hinck, A. P.; Ishima, R. *J. Biomol. NMR* **2007**, *38*, 315–324.
- Ferrage, F.; Piserchio, A.; Cowburn, D.; Ghose, R. *J. Magn. Reson.* **2008**, *192*, 302–313.
- Farrow, N. A.; Muhandiram, R.; Singer, A. U.; Pascal, S. M.; Kay, C. M.; Gish, G.; Shoelson, S. E.; Pawson, T.; Forman-Kay, J. D.; Kay, L. E. *Biochemistry* **1994**, *33*, 5984–6003.
- Goldman, M. *J. Magn. Reson.* **1984**, *60*, 437–499. Kumar, A.; Grace, R. C. R.; Madhu, P. K. *Prog. NMR Spectrosc.* **2000**, *37*, 191–319.
- Renner, C.; Schleicher, M.; Moroder, L.; Holak, T. A. *J. Biomol. NMR* **2002**, *23*, 23–33.
- Levitt, M. H.; Freeman, R.; Frenkiel, T. *J. Magn. Reson.* **1982**, *47*, 328–330. Skelton, N. J.; Palmer, A. G.; Akke, M.; Kordel, J.; Rance, M.; Chazin, W. J. *J. Magn. Reson., Ser. B* **1993**, *102*, 253–264.
- Markley, J. L.; Horsley, W. J.; Klein, M. P. *J. Chem. Phys.* **1971**, *55*, 3604–&.
- Levitt, M. H.; Di Bari, L. *Bull. Magn. Reson.* **1993**, *16*, 94–114.
- Levitt, M. H.; Di Bari, L. *Phys. Rev. Lett.* **1992**, *69*, 3124–3127. Ghose, R. *Concepts Magn. Reson.* **2000**, *12*, 152–172.
- Morris, G. A.; Freeman, R. *J. Magn. Reson.* **1978**, *29*, 433–462.
- Akke, M.; Brüschweiler, R.; Palmer, A. G., III. *J. Am. Chem. Soc.* **1993**, *115*, 9832–9833. Tugarinov, V.; Liang, Z. C.; Shapiro, Y. E.; Freed, J. H.; Meirovitch, E. *J. Am. Chem. Soc.* **2001**, *123*, 3055–3063. Massi, F.; Palmer, A. G. *J. Am. Chem. Soc.* **2003**, *125*, 11158–11159.

JA809526Q